WIND PROFILES, MOMENTUM FLUXES AND ROUGHNESS LENGTHS AT CABAUW REVISITED

J. W. Verkaik (job.verkaik@knmi.nl)
Royal Netherlands Meteorological Institute, De Bilt, The Netherlands

A. A. M. Holtslag (bert.holtslag@wur.nl)
Wageningen University, Meteorology and Air Quality Section, Wageningen, The Netherlands

Abstract. This paper describes the results of a measuring campaign focusing on wind speed and momentum fluxes in the atmospheric boundary layer up to 200 m. The measurements were conducted in 1996 at the Cabauw site in the Netherlands. Momentum fluxes are measured using the K-Gill Propeller Vane. Estimates of the roughness length are derived using various techniques from the wind speed and flux measurements, and the observed differences are explained by considering the source area of the meteorological parameters. A clear rough-to-smooth transition is found in the wind speed profiles at Cabauw. The internal boundary layer reaches the lowest k-vane (20 m) only in the south-west direction where the obstacle-free fetch is about 2 km. The internal boundary layer is also reflected in the roughness lengths derived from the wind speed profiles. The lower part of the profile (< 40 m) is not in equilibrium and no reliable roughness analysis can be given. The upper part of the profile can be linked to a large-scale roughness length. Roughness lengths derived from the horizontal wind speed variance and gustiness have large footprints and therefore represent a large-scale average roughness. The drag coefficient is more locally determined but still represents a large-scale roughness length when it is measured above the local internal boundary layer. The roughness length at inhomogeneous sites can therefore be determined best from drag coefficient measurement just above the local internal boundary layers directly, or indirectly from horizontal wind speed variance or gustiness. In addition the momentum and heat flux along the tower are analyzed and these show significant variation with height related to stability and possibly surface heterogeneity. It appears that the dimensionless wind speed gradients scale well with local fluxes for the variety of conditions considered, including the unstable cases.

Keywords: Drag coefficient, Cabauw, Flux-profile relationship, Footprint area, Gustiness, K-Gill, Local scaling, Roughness, Wind

1. Introduction

This paper describes an experiment set up to further investigate profiles of wind speed, fluxes, flux-profile relationships, and roughness lengths at relatively high altitudes in the atmospheric boundary layer (ABL) at Cabauw (The Netherlands). The 213-m high tower offers excellent

opportunities for boundary-layer research and many studies have been done on the roughness and flux-profile relationships (Van Ulden and Wieringa, 1996; Beljaars and Bosveld, 1997). Nieuwstadt (1978) fitted profiles of wind speed and temperature measured along the tower to the flux-profile relationships. In the west direction, the most open sector at Cabauw, he found large discrepancies between the fluxes from the profiles and direct flux measurements. Beljaars (1982) showed that about half of the momentum flux can be attributed to form drag on the wind breaks in the Cabauw environment. Close to the tower the surface is free of obstacles. Consequently, momentum fluxes close to the surface are lower than those aloft and the local roughness length is much smaller than the large-scale roughness length.

Using a small data set Beljaars et al. (1983) showed that the momentum flux increases 40% between 3.5 and 22.5 m for wind directions with wind breaks in the upstream terrain. The dimensionless wind speed gradient in the lowest 10 m is closer to literature values when it was increased by 40% for those directions. Nieuwstadt (1984) used Cabauw data and showed that in stable boundary-layers the dimensionless gradient scales with the local fluxes of momentum and heat instead of the surface fluxes. Holtslag (1984) estimated the momentum and heat flux at the surface from data that are available at standard synoptic stations. He estimated wind speed profiles up to 200 m and compared them to observations at the tower. Beljaars (1987b) estimated the large-scale roughness lengths from observations of the standard deviation of the horizontal wind speed in the surface layer and found values between 0.04–0.15 m depending on wind direction.

In the present study we elaborate on the results of Beljaars et al. (1983), however, our data set is much larger. We investigate whether the flux-profile relationships are valid in the disturbed boundary-layer and explore the use of local scaling in stable and unstable conditions. Note that only few papers deal with the validation of local scaling of wind and temperature gradients in unstable conditions. Sorbjan (1986) tested local scaling for the dimensionless wind speed (ϕ_m) and temperature gradient (ϕ_h) using a small data set from Minnesota. Yumao et al. (1997) tested local scaling for ϕ_m and ϕ_h for an urban and a rural site near Nanjing. Recently, Steeneveld et al. (2005) tested local scaling at Cabauw for temperature and humidity profiles.

In this paper we test local scaling for ϕ_m at Cabauw. Although the landscape at Cabauw is fairly open, there are frequent wind breaks and scattered villages causing a strong disturbance of the surface layer (Beljaars, 1982). The density and distance of the disturbances is different for different wind directions. In addition, we compute the surface roughness using several methods. We investigate how the roughness

Table I. Instrumentation at the Cabauw tower during the summer of 1996.

Element	Height (m)	Direction	Instrument
Temperature	0.6, 1.5, 10, 20, 40, 80, 140, 200	south-east	Thermocouple (melting ice reference at 0.6 and 200 m)
Wind	10, 20, 40, 80, 140, 200	south-west, north	Propeller vane (Gill 8002DX)
Momentum and heat fluxes	20, 100, 180	south-west, north	K-Gill propeller vane (Young 35301)

lengths relate to the fluxes, wind speed profiles and their footprint areas. We re-evaluate the results of Nieuwstadt (1978) and explain the discrepancies he observed between momentum fluxes from profiles and direct flux measurements. Our flux measurements include momentum and sensible heat fluxes. In this paper we focus on the wind speed profile and momentum flux. We present the results of the summer period (May–October). During this period wind conditions were close to their climatological normals.

2. Experiment

The Royal Netherlands Meteorological Institute (KNMI) has conducted ABL observations at the Cabauw site since the early seventies. The tower is a solid cylinder with 2 m diameter. It is 213 m high and has booms in three direction (10°, 130°, 250°) at intervals of 20 m. The booms extend 9.4 m beyond the surface of the cylinder. At the end of the north and south-west pointing booms two lateral extensions (1.5 m) carry four plugs. The routine observations include profiles of meteorological parameters (e.g. wind speed and direction, temperature, moisture) and a number of surface parameters (e.g. radiation, precipitation). Table I gives details on the installed instruments (Monna and Van der Vliet, 1987; Van der Vliet, 1998).

From the routine surface layer observations the friction velocity and sensible heat flux are computed using the flux-profile relationships for homogeneous terrain (Dyer, 1974). These observations are referred to as the surface layer observations of $u_{*\mathrm{SL}}$ [m s^{-1}] and H_{SL} [W m^{-2}] in this paper. H_{SL} and $u_{*\mathrm{SL}}$ are computed from the wind speed at 10 m, a tabulated effective roughness length relevant for the particular

wind direction, and the difference in temperature between 1.5 and 10 m (Wessels, 1984).

The roughness length ($z_{0\mathrm{std}}$, [m]) has been derived from the ratio of the standard deviation of the longitudinal wind speed variations (σ_u) to the wind speed in 10-min averaging periods measured during neutral conditions at 10 m height (Beljaars, 1987a; Beljaars, 1988). From $u_{*\mathrm{SL}}$ and H_{SL} the surface layer stability parameter (Obukhov length) is calculated from $L = -u_*^3 \theta c_p \rho / \kappa g H$. Here θ is the temperature [K], ρc_p is the product of the specific heat and density of air [J K^{-1} m^{-3}], and g is the acceleration of gravity [m s^{-2}].

In 1996 the routine measurements were completed with direct flux measurement at the tower. K-Gill Propeller Vanes were used to measure momentum and sensible heat fluxes. The k-vane is an instrument comprising two propellers, one oriented 45° upward, the other 45° downward, and a vane to aim the propellers into the main wind direction. They have been equipped with a thermocouple to measure the heat flux. The k-vane is a first order response instrument with a response length of 2.9 m. Details on the k-vane can be found in Verkaik (1998). The averaging period is 30 minutes for both the k-vane measurements and the routine Cabauw measurements. Data on the atmospheric boundary layer (ABL) height is not available for the major part of our data set.

Wind speed measurements at the tower suffer from flow distortion. For that reason two anemometers are placed at each level, one on the north (on the most right plug of the right lateral extension) boom and one on the south-west boom (on the most left plug on the left lateral extension). The anemometer which is best exposed is used in the analysis. At 20 m and below the building at the base of the tower causes flow distortion as well (Wessels, 1983). The octagonal shaped building is 3.8 m high and has a diameter of 17.3 m. For that reason the wind speed measurements at 10 and 20 m are not measured at the main tower but at auxiliary masts 29 m in south-east and 73 m in the north-west direction of the main tower. However, the flux measurements at 20 m are done at the main tower. Comparison of the momentum and heat flux measurements at each level as function of wind direction shows that the flow distortion by the tower and the building does not affect the flux measurement significantly, not even at the 20-m level.

When planning the measurement campaign the k-vanes were preferred to sonic 3-D anemometers as they were considered better all-weather flux probes and, at that time, a cheaper alternative. The measurements continued throughout the summer of 1996. Due to frequent malfunctioning of the k-vane's electronics, however, the data set has many gaps.

Figure 1. Roughness lengths in gray scale for the Cabauw environment [$(10\ \mathrm{km})^2$]. The circle in the center of the figure indicates the tower position. Dark areas are smooth, bright areas are rough. Lowest and highest roughness lengths found in this region are approximately 0.001 and 1 m respectively. Pixel size $(25\ \mathrm{m})^2$.

3. Terrain description

The Cabauw tower is situated in the central river delta in the south-western part of the Netherlands (52°58'18" N, 4°55'37" E). It is surrounded by meadows (> 80% grass). The North Sea is about 50 km away in the north-west direction. Close to the tower the surface consists mainly of short grass with several small villages, scattered farms, rows of trees and bushes. Maps of the Cabauw environment have been published in Holtslag (1984), Monna and Van der Vliet (1987), and Van Ulden and Wieringa (1996).

A map of the roughness in the Cabauw environment is plotted in Figure 1. The roughness map is derived from the land-use map LGN3+ of the Dutch environmental research institute Alterra (De Wit et al., 1999). LGN3+ is a raster file covering the whole of the Netherlands with a resolution of $(25\ \mathrm{m})^2$. LGN3+ is derived from Landsat-TM satellite images from 1995 and 1997 and topographical information. Over forty land use types are distinguished of which 15 are present in the Cabauw environment. Despite the high resolution of the LGN3+-images, narrow roughness elements like tree lines may not be distinguished. For example, most roads in the Cabauw environment are lined with trees which are rarely detected. Even so, complex terrain features, like the river-

Table II. Wind direction sectors for Data Analysis.

north	315°–45°	regularly spaced wind breaks, 1–2 km spacing, on pasture making a *shelterbelt landscape*
east	45°–105°	a chain of small villages making up a *uniform rough* landscape
south	105°–165°	orchards, dikes and the river bed making up a rather complex, *scattered rough* terrain
west	180°–240°	*nearly smooth, open* landscape

Table III. Data selection rules, number of 30-min runs, and percentages of data coverage. U: wind speed, θ: temperature, and dd: wind direction.

Total	8832	100%
$U_{\mathrm{SL},20} \geq 3$ m s^{-1}	6163	70%
$\theta_{\mathrm{SL},20}$ and $D_{\mathrm{SL},20}$ present	5503	62%
no precipitation	5092	58%
$u_{*\mathrm{SL}}$ present	4835	55%
dd within selected directions	3670	42%
$U_{\mathrm{kv}} \geq 3$ m s^{-1} at each height	≈ 2500	$\approx 30\%$

banks, are not recognized. To each land-use type a roughness length adopted from literature is assigned (Wieringa, 1993). Note that these roughness lengths usually refer to homogeneous areas, while they are applied to inhomogeneous terrain here.

Figure 1 shows that southwest of the tower is the only sector that is open and nearly free of obstacles for several kilometers. To the north there is a road with houses and trees comprising a windbreak-like obstacle at a minimum distance to the tower of about 0.5 km. Farther upstream pasture continues until again there is a road with houses and trees at about 3 km. To the east is the village Lopik at a distance of 1 km. In this direction the local road continues and so do the built-up areas and trees. To the southeast lies a complex terrain with roads, orchards, and the river bed. From inspection of the land-use map four wind direction sectors are distinguished for the Cabauw site (see Table II). The data set will split up in these wind direction sectors to assess the influence of differences in the upstream terrain on the profiles and fluxes.

Table IV. Stability Classes for Data Analysis.

1.	Unstable		$L^{-1}<$	$-(200\ \mathrm{m})^{-1}$
2.	Slightly Unstable	$-(200\ \mathrm{m})^{-1}\leq$	$L^{-1}<$	0
3.	Slightly Stable	$0\ <$	$L^{-1}\leq$	$(200\ \mathrm{m})^{-1}$
4.	Stable	$(200\ \mathrm{m})^{-1}\ <$	L^{-1}	

4. Data set

As the k-vanes need some wind to operate properly, only those cases are selected where the wind speed measured at 20 m by the tower and the k-vanes at all levels is equal to or larger than 3 m s^{-1}. Runs with significant precipitation are also excluded, *i.e.* the amount of precipitation is less than 0.1 mm, and the duration is less than 1 min per 30-min interval. Next the routine measurements of the wind direction and temperature at 20 m and the friction velocity must be available.

Table III shows how the number of 30-min runs available for analysis is reduced by the selection rules. While the highest possible number of 30-min runs in the summer period is 8832, about 2500 momentum flux runs (30% data coverage) and 2000 heat flux runs (25%) are available for analysis at each level. For the determination of the roughness lengths the following addition criteria are used to exclude cases with shallow boundary layers (Korrell et al., 1982): wind direction turning with height is less than 20°, the friction velocity is larger than 0.15 m s^{-1}, and the wind speed gradient must be positive.

The surface layer Obukhov length (L) has been used to split up the data set in four stability classes (see Table IV). The distribution of the runs over the stability and wind direction classes is given in Table V and VI. Table V and VI show that stable conditions prevailed during the measuring campaign. The number of runs in the east sector is substantially less than for the other sectors.

To determine at what time of day the selected stability subsets are taken, $\cos(2\pi\ \mathrm{time}/2400)$ and $\sin(2\pi\ \mathrm{time}/2400)$ are averaged for each subset. The phase angle of the resulting vector indicates the preferential time and its length is a measure for this preference. In case all events would occur at the same time the vector would have unity length, in case the events would be randomly distributed over time the vector would a length close to zero. For all k-vane heights and wind direction sectors together the results are (1146, 0.77) for unstable, (1236, 0.58) for slightly unstable, (2140, 0.14) for slightly stable and (2307, 0.57) for stable conditions. It is clear that the (slightly) unstable subset comprises

Table V. Numbers of 30-min runs for the analysis of the momentum flux.

Stability class	Height (m)	Wind direction sector				
		1	2	3	4	All sectors
Unstable	20	260	39	121	210	630
	100	315	33	124	214	686
	180	247	60	110	98	515
	All heights	822	132	355	522	1831
Slightly unstable	20	227	82	45	177	531
	100	243	12	44	161	460
	180	198	85	42	104	429
	All heights	668	179	131	442	1420
Slightly stable	20	113	93	26	213	445
	100	141	5	27	177	350
	180	109	98	27	130	364
	All heights	363	196	80	520	1159
Stable	20	231	167	318	357	1073
	100	295	118	299	371	1083
	180	250	211	308	262	1031
	All heights	776	496	925	990	3187
	Totals	2629	1003	1491	2474	7597

many samples takes round or before noon. It can be expected that the ABL is shallow and rapidly growing. In those cases the selection of wind speeds larger than 3 m s^{-1} favors conditions with strong entrainment (Driedonks and Tennekes, 1984; Pino et al., 2003). The stable subset is dominated by samples taken round midnight and the slightly stable subset has a small surplus of samples taken in the early evening.

In addition to the selection criteria listed above, we have also used the criteria given by Korrell et al. (1982) to identify the measurements taken in the surface layer. This confirmed that especially in stable conditions at 100 and 180 m a large number of the observations is actually above the surface layer.

Malfunction of the k-vanes has been a serious problem. The main cause for this has been frequent breakdown of the electronics in the photochopper of the propeller. Although the exact reason never became clear, it is probably due to atmospheric electricity. At our demand the Young company replaced the plastic propeller shafts by stronger metal shafts. Because of this atmospheric electricity could be conducted

Table VI. Numbers of 30-min runs for the analysis of the sensible heat flux.

Stability class	Height (m)	Wind direction sector				
		1	2	3	4	All sectors
Unstable	20	225	33	78	113	479
	100	315	28	106	200	649
	180	217	36	89	91	433
	All heights	787	97	273	404	1561
Slightly unstable	20	220	82	38	101	441
	100	243	10	44	155	452
	180	153	76	36	102	367
	All heights	616	168	118	358	1260
Slightly stable	20	111	93	21	149	374
	100	141	4	26	173	344
	180	88	96	22	130	336
	All heights	340	193	69	452	1054
Stable	20	219	164	210	228	821
	100	295	100	286	351	1032
	180	190	147	262	244	843
	All heights	704	411	758	823	2696
	Totals	2447	869	1218	2037	6571

into the photochopper electronics. Later during the experiment spark bridges were used in the photochopper unit and after that this failure occurred less often. Other causes of drop-out were short-circuit in the thermocouple amplifiers, broken thermocouples by rain or hail and computer failure.

5. Wind profiles and Fluxes

Profiles of wind speed (U), normalized with the wind speed at 200 m are plotted in Figure 2 for all wind direction sectors and stability classes. Per wind direction sector and stability class each measuring point comprises at least 5 runs (usually much more). The ratio (R) of the wind speed at height z to that at 200 m has been calculated by fitting the equation $U_z = R \times U_{200}$ using a χ^2-procedure. The uncertainty in U is assumed to be 10% in this analyses, with the uncertainty of the 10% percentile wind speed in the data set as a minimum.

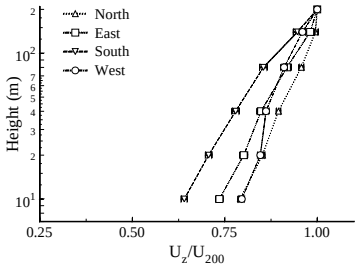

a. Unstable, $1/L < -0.005$ m^{-1}

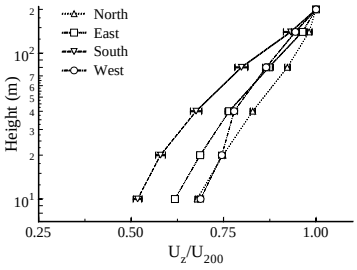

b. Slightly unstable, -0.005 m^{-1} $< 1/L < 0$

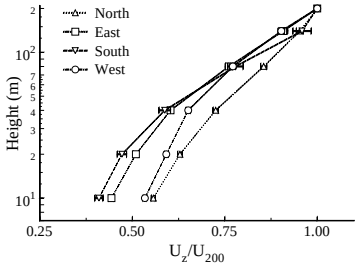

c. Slightly stable, $0 < 1/L < 0.005$ m^{-1}

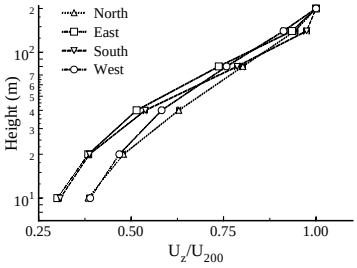

d. Stable, $1/L > 0.005$ m^{-1}

Figure 2. Scaled wind speed profiles. U_z has been scaled by U_{200} (routine Cabauw measurement).

From the velocity profiles it can be seen that the retardation of the wind speed is the strongest in the south sector and not in the east sector, which is usually considered to be the roughest sector. In the north sector the retardation is comparable to that of the west sector, which is considered to be the smoothest. Also evident is the strong curvature in these profiles, especially in stable conditions. At 40 m, in (slightly) unstable and slightly stable conditions a knee in the velocity profile can be seen in the west sector suggesting a rough-to-smooth transition in surface roughness.

Ratios of friction velocity measured by k-vanes to that of the surface layer are plotted in Figure 3. In the unstable, well mixed, ABL $u_{*\mathrm{kv}}$ is close to $u_{*\mathrm{SL}}$ and can be considered approximately constant with height. The relative momentum flux divergence increases with increasing stability. In the stable ABL u_* at 180 m has decreased to 50% of its surface value. The divergence is probably due to the finite depth of the ABL. In the east direction $u_{*\mathrm{kv}}$ at 20 m is larger than $u_{*\mathrm{SL}}$ for

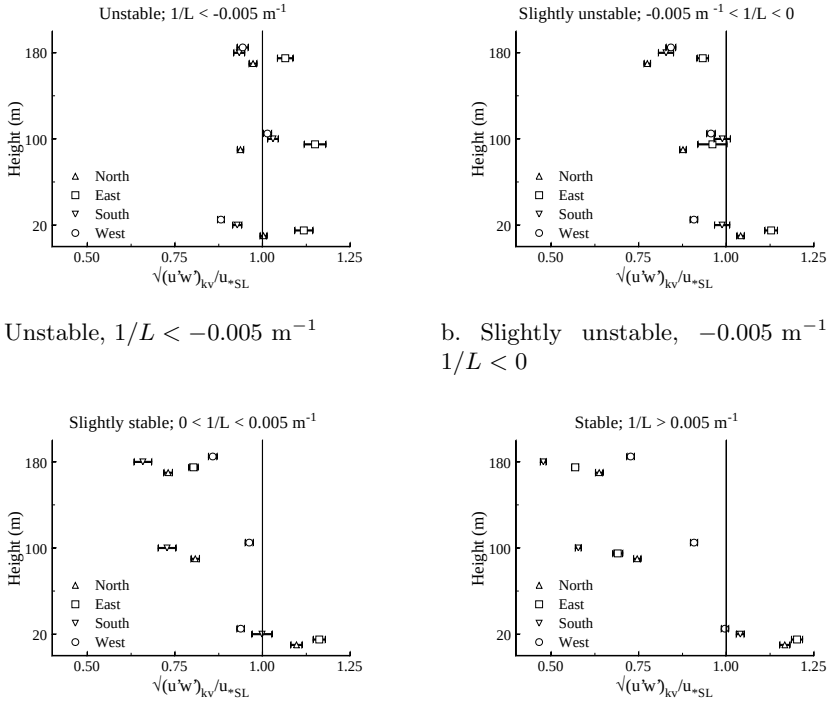

a. Unstable, $1/L < -0.005$ m^{-1}

b. Slightly unstable, -0.005 m^{-1} $< 1/L < 0$

c. Slightly stable, $0 < 1/L < 0.005$ m^{-1}

d. Stable, $1/L > 0.005$ m^{-1}

Figure 3. Friction velocity as measured by the k-vanes normalized with the surface layer friction velocity.

all stabilities. In this direction the upstream fetch is heavily disturbed close to the tower. This is reflected by the $u_{*\mathrm{kv}}$-measurements, while $u_{*\mathrm{SL}}$ represents a large-scale friction velocity. In west and in the south direction $u_{*\mathrm{kv}}$ is smaller than $u_{*\mathrm{SL}}$ at 20 m. In these directions there are few obstacles in the towers vicinity.

In general Monin-Obukhov similarity theory is based on the assumption that momentum and heat fluxes do not change throughout the surface layer, and the surface layer is defined as the 'constant flux layer'. Figure 3 shows that there is a strong momentum flux divergence, except for the unstable cases. A strong divergence was also found for the sensible heat flux (Figure 4). The daytime flux divergence (unstable conditions) may partially be caused by entrainment. The data selection excludes low wind speed and consequently low u_*-values to ensure that the k-vanes are operating properly. Moreover, the data set includes many situations with unstable, shallow boundary layers in the early morning hours with a growing convective boundary layer. These condi-

tions are in favor of strong entrainment and the entrainment heat flux can be about 20–50% of the surface heat flux (Driedonks and Tennekes, 1984; Pino et al., 2003). With an ABL-height of 500 m the heat flux may become zero at a height of only 400 m. The application of the surface layer criteria of Korrell et al. (1982) indicates that indeed the ABL has often been shallow and a significant portion of the measurements are done above the surface layer, where the momentum and heat fuxes are expected to decrease. Under such conditions we can not expect that Monin-Obukhov similarity theory is still applicable.

Let us explore the dimensionless wind speed gradient using $\partial U/\partial z$ from the tower measurements:

$$\phi_m \left(\frac{z}{L} \right) = \frac{kz}{u_*} \frac{\partial U}{\partial z}. \tag{1}$$

Here we analyze our data by using both the local values for u_* and L (so called local scaling) as well as the surface layer values for u_* and L. Since the fluxes become smaller with height and the scatter increases as well, only the k-vane fluxes at 20 and 100 m are analyzed. Following Nieuwstadt (1984) the wind speed profile is fitted to the function $U = a_1 + a_2 z + a_3 z^2 + a_4 \ln z$. From this fitted profile $\partial U/\partial z$ is computed at 20 or 100 m. The averages of z/L and ϕ_m are plotted in Figs. 5a and 5c for the surface layer scaling results. The data have been averaged in bins each containing 20 runs. The standard deviation of the mean of ϕ_m has been plotted as error bar. For comparison Dyer's (1974) stability function is also plotted. In addition to the usual data selection, positive wind speed gradients were required ($\partial U/\partial z > 0$), and cases with $u_* < 0.15$ m s^{-1} were rejected to ensure that ϕ_m is well defined.

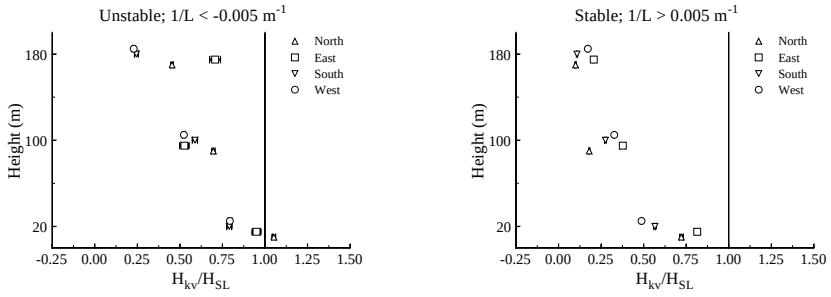

a. Unstable, $1/L < -0.005$ m^{-1} b. Stable, $1/L > 0.005$ m^{-1}

Figure 4. Sensible heat flux as measured by the k-vanes normalized with the surface layer heat flux.

At 20 m ϕ_m is lower than Dyer's curve. Only in the south direction, the most complex and rough sector, in unstable conditions ϕ_m is larger than Dyer's curve. With increasing stability the difference between ϕ_m and Dyer's curve increases. At 100 m there are less measuring points, especially in the east sector there are few. The scatter in the data is also larger. In all directions ϕ_m has increased compared to the 20-m level. In the north and west direction ϕ_m is still close to Dyer's curve for neutral and unstable cases. In the south sector ϕ_m is far above Dyer's curve over the whole range of stabilities.

In Equation (1) u_* and L can also be computed from the k-vane measurements (local scaling). As shown in Figs. 5b and 5d local scaling reduces the scatter in ϕ_m considerably. At both 20 and 100 m ϕ_m collapses to a single curve, also for the south sector. In neutral and unstable cases ϕ_m is still below Dyer's curve at 20 m. Although the fluxes at 20 m are still close to their surface layer values, Fig. 5b shows that local scaling performs slightly better, especially in stable cases. Figure 5d shows that at 100 m local scaling performs much better than surface layer scaling. Figs. 3a and 4a show that at 100 m the difference between surface-layer scaling and local scaling is primarily caused by the difference in heat flux.

Note that ϕ_m and z/L both contain the factor $\kappa z/u_*$ (see Equation (1)). Consequently the correlation that is found in Figure 5 may partially be an artifact. In Figure 6 dU/dz is plotted against $(u_*/\kappa z)(z/L) = \kappa u_*/L = (g/\theta)\overline{w'\theta'}/u_*^2$ for the 100-m level for surface layer- and local scaling. This way of plotting is free of artificial correlation. Figure 6 confirms that the good performance is not artificial and that there is less scatter when local scaling is used.

6. Roughness lengths

In this section several methods to determine the aerodynamic roughness length (z_0) are compared. The roughness length can be computed from wind speed profiles, gustiness analysis, and the drag coefficient. All these methods may result in different estimates of z_0 as they have different source areas.

The footprint or source area is the surface effectively determining the level or gradient of a meteorological parameter downstream. It can be described by sophisticated weighting functions and is a function of height, stability, and roughness itself. In neutral conditions the area with the maximum contribution lies upwind at a distance of about ten times the measuring height. The width of the source area is about 20°–30°. Atmospheric instability shrinks the source area and makes it come

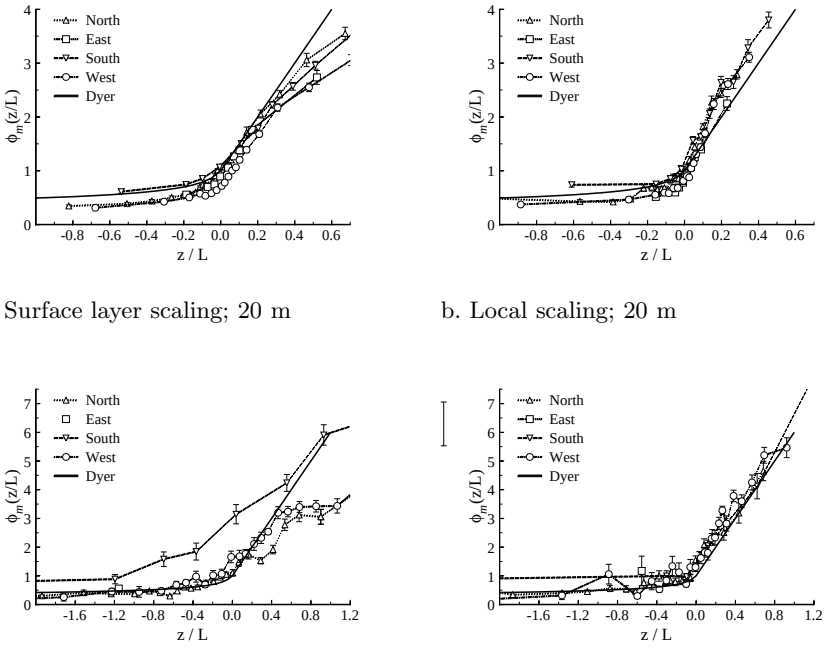

a. Surface layer scaling; 20 m

b. Local scaling; 20 m

c. Surface layer scaling; 100 m

d. Local scaling; 100 m

Figure 5. Dimensionless wind speed gradients calculated from k-vane fluxes at 20 and 100 m for the four wind direction sectors. Note that u_* and L are calculated from the surface layer fluxes (a and c), and from the fluxes measured by the k-vane itself (b and d).

closer (Van Ulden, 1978; Schmid and Oke, 1990; Horst, 1999; Schmid and Lloyd, 1999; Kljun et al., 2004).

The larger the source area of a meteorological parameter, the more this entity will represent a large-scale average. The largest eddies in the ABL are also those that adapt slowest of all to changes in surface properties (Højstrup, 1981; Beljaars, 1987b). The longitudinal velocity variance in the surface layer (σ_u^2) is mostly determined by the largest eddies. For that reason $z_{0\mathrm{std}}$ represents the best large-scale average of all roughness lengths.

6.1. Roughness lengths from Profiles

Using Nieuwstadt's (1978) method the wind speed profile at Cabauw is analyzed as function of wind direction. Nieuwstadt minimized the function

$$\Phi\left(u_*, \theta_*\right) \;=\; \Phi_u/\Delta u^2 + \Phi_\theta/\Delta\theta^2, \quad \text{where} \tag{2}$$

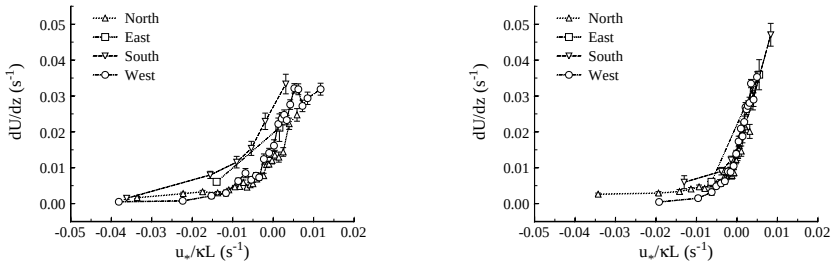

a. Surface layer scaling; 100 m b. Local scaling; 100 m

Figure 6. As Figure 5 but now for the wind speed gradient dU/dz versus $u_*/\kappa L$. In this plot any artificial correlation is avoided.

$$\Phi_u = \sum_{i=2}^{N_U} \Big[U_{z_i} - U_{z_{\rm ref}} - u\left(z_i, u_*, \theta_*\right) + u(z_{\rm ref}, u_*, \theta_*) \Big]^2, \quad (3)$$

and

$$\Phi_\theta = \sum_{j=2}^{N_\theta} \Big[\theta_{z_j} - \theta_{z_{\rm ref}} - \theta(z_j, u_*, \theta_*) + \theta(z_{\rm ref}, u_*, \theta_*) \Big]^2. \quad (4)$$

Here Δu and $\Delta\theta$ are the measuring errors in the wind speed U and temperature θ respectively, and $\theta_* = -H/\rho c_p u_{*\rm prof}$ is the temperature scale, where $u_{*\rm prof}$ is the profile derived friction velocity, $u(z, u_*, \theta_*)$ and $\theta(z, u_*, \theta_*)$ are the log-linear functions for wind speed and temperature and N_U and N_θ are the number of heights at which wind speed temperature are measured respectively. The subscript 'ref' refers to the lowest level used in the profiles. Nieuwstadt used estimates of z_0 and added $U\left(z_0\right) = 0$ to his profile. We will not do so, as the profiles are used to determine z_0. Dyer's (1974) stability functions and the integrated log-linear functions Ψ_M and Ψ_H as presented by Garratt (1992) are adopted here. For U the total horizontal wind vector has been used. The fitted wind speed profile is extrapolated to $U(z_0) = 0$ to derive the roughness length. Any zero plane displacement, which is expected to be small and of minor importance when computing z_0, is neglected (Nieuwstadt, 1978; Kustas and Brutsaert, 1986; Grant and Mason, 1990; Grant, 1991). In addition to the basic selection criteria, we applied the criteria of Korrell et al. (1982) as well, to ensure all profiles were within the surface layer and we analyzed only the slightly unstable cases.

In Figure 7a the resulting roughness lengths $z_{0\rm prof}$ are plotted. It is computed using two different height intervals: 10–40 m and 40–200 m. Every point represents the average over 30 estimates of $z_{0\rm prof}$. For

comparison $z_{0\mathrm{std}}$ is plotted as well. Figure 7a shows that the higher profile yields similar roughness lengths to $z_{0\mathrm{std}}$ in most directions where, apparently, the 40-m level is not influenced by the rough to smooth transition close to the tower for those directions. Only in the south-west sector $z_{0\mathrm{prof}}$ drops to values that are far too low to be realistic. In this direction the roughness length is smaller than 1 mm. Such small roughness lengths can only be found over very smooth surfaces (water, sand, snow covered land). This indicates that the profiles in this sector at Cabauw are strongly disturbed. The lower profile yields smaller roughness lengths than the higher profile except for the sectors from west to north. This profile also yields very low z_0-values in the south-west direction. In most directions the free fetch is not long enough, less than a few hundreds of meters, to accelerate the 10-m wind. However, in the south-west direction the fetch is longer (0.5–2 km), resulting in a very low estimate of $z_{0\mathrm{prof}}$. The low $z_{0\mathrm{prof}}$ in the upper profile shows that the local IBL has reached the 40-m level in the direction 240°. The unrealistically low z_0-values in the lower profile, however, show that the equilibrium boundary layer has not yet reached the 40-m level in this direction. Figure 7a also shows that directions with distinct roughness values can be very narrow. This indicates that the source areas for these measurements are very narrow as well.

6.2. Roughness lengths from the drag coefficient

The drag coefficient, $C_d \equiv (u_*/U)^2$, can be used to estimate the roughness length using the logarithmic wind speed profile. From the logarithmic wind speed profile it follows that C_d is a function of z, z_0, and stability:

$$\sqrt{C}_d = \frac{\kappa}{\ln z/z_{0\mathrm{drag}} - \Psi_M\left(z/L\right) + \Psi_M\left(z_{0\mathrm{drag}}/L\right)}. \tag{5}$$

An advantage of this approach is that measurements need to be done only at a single level. A disadvantage is the need for measurements or estimates of the momentum flux. Fortunately, u_* can be estimated from σ_u or the gustiness. Both can be assessed by regular anemometers. The routine Cabauw roughness length as shown in Figure 7a is an example of the application of this method. Gustiness records have been available since the early seventies at most Dutch wind stations. These records proved very useful in wind climate research to monitor the quality of stations (Wieringa, 1976; Verkaik, 2000).

From the present data set the roughness lengths found from direct observations of u_*/U or the gustiness can be compared to those from σ_u. The gustiness derived roughness length ($z_{0\mathrm{gust}}$) has been calculated

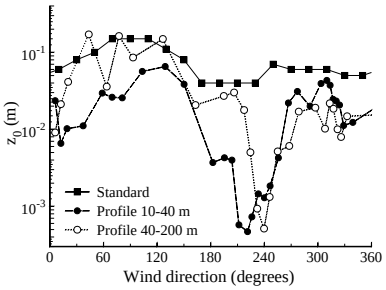

a. Roughness lengths from profile measurements using different height intervals compared to $z_{0\mathrm{std}}$.

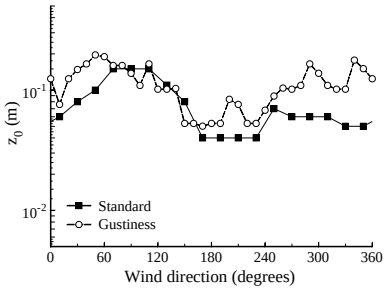

b. Roughness lengths from gustiness measurements at 10 m compared to $z_{0\mathrm{std}}$.

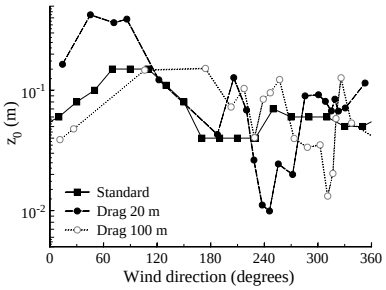

c. Roughness lengths from the drag coefficient measurements at 20 m and 100 m compared to $z_{0\mathrm{std}}$.

Figure 7. Roughness lengths estimated using various methods at the Cabauw site.

using the routine measurements at 10 m per 10°-wide bins. In Figure 7b $z_{0\mathrm{gust}}$ is plotted and compared to $z_{0\mathrm{std}}$. For most directions $z_{0\mathrm{gust}}$ is similar or larger than $z_{0\mathrm{std}}$. Compared to $z_{0\mathrm{prof}}$ it shows very little directional variation.

Using the k-vane measurements at 20 and 100 m $z_{0\mathrm{drag}}$ has been calculated. The same data selection as for the profiles has been done. In Figure 7c $z_{0\mathrm{drag}}$ is plotted. The directional variation in $z_{0\mathrm{drag}}$ is larger than that of $z_{0\mathrm{std}}$ and $z_{0\mathrm{gust}}$. It is possible to indicate the surface features causing the profile of $z_{0\mathrm{drag,\ 20m}}$. The peak in the north-east direction is caused by farms and trees at 300 m distance. The peak at 190° is caused by trees and orchards (0.5–1.5 km). A little more to the south of that there is a small window overlooking the river bed. This is a very smooth area. In the south-west direction roughness lengths in the order of centimeters are found. This roughness length corresponds

to that of grassland and this direction is also the direction with the largest free fetch over grassland.

At 100 m $z_{0\mathrm{drag}}$ is in the range 0.01–0.10 m for most directions. The 100-m roughness length shows a noisy profile in the west directions. However, assuming that the 100-m observation are not influenced by the closest windbreaks, the low z_0 in direction 300° coincides with a very smooth upwind fetch starting $\simeq 1$ km from the tower (see Figure 1). The low z_0 in the north direction, however, cannot be explained easily. In the east direction z_0 is clearly smaller at 100 m than at 20 m, indicating that the 100-m footprint is mainly overlooking the village Lopik in the east.

7. Discussion

7.1. Flux-profile relationships

At 20 m ϕ_m is lower than Dyer's curve in most directions when using surface layer scaling. When using local scaling in unstable cases ϕ_m is lower as well. A low ϕ_m indicates that $\partial U/\partial z$ is small compared to u_*, typical for situations after a rough-to-smooth change (Rao et al., 1974). Figure 5a can be compared with figures 5 and 7 from Beljaars et al. (1983) where also low values for ϕ_m were found.

Deviations of the regular flux-profile relationships in very stable conditions using surface layer scaling have been observed frequently. Local scaling has been more successful in these cases (Holtslag and Nieuwstadt, 1986; Holtslag and De Bruin, 1988; Beljaars and Holtslag, 1991; Vickers and Mahrt, 1999). Local scaling can also be applied to ϕ_m in unstable condition at homogeneous sites (Sorbjan, 1986; Yumao et al., 1997). Figure 5b and 5d however, show that local scaling of ϕ_m also applies in the disturbed boundary layer at Cabauw. If the underestimation of ϕ_m at 20 m is explained by the rough-to-smooth transition, then Figure 5d shows that at 100 m the flux-profile relationships seem to reflect an equilibrium ABL as long as local scaling is applied.

Comparing eddy-correlations measurements at 3.5 and 22.5 m Beljaars et al. (1983) found that there is an increase in friction velocity with height, except for those directions which are really free of obstacles. Heat and moisture fluxes are about the same at both levels for all directions. These observation confirmed the assumptions of Beljaars (1982), firstly, the heat flux throughout the surface layer is constant in spite of perturbed profiles, and, secondly, the exchange coefficients for momentum and heat are modified in the same way by obstructions. The success of local scaling suggests that these reasonings still hold at 100 m and despite the strong flux divergence.

Our data selection for unstable conditions is in favor of situations with developing boundary layers in the morning hours in combination with wind shear. The strong heat flux divergence in unstable conditions indicates that the boundary layer is heating up (Figure 4). Moreover, the entrainment rate is expected to be relatively high (Pino et al., 2003), so the heat flux becomes negative at a relatively low height. Whereas the heat flux becomes negative by entrainment in the upper part of the ABL, the momentum flux is enhanced. This explains why, in contrast to the heat flux, there is little divergence in momentum flux (Figure 3).

7.2. Wind speed profiles and Local roughness

The rough-to-smooth transition at Cabauw causes a knee in the wind speed profile. The knee is best seen in the west sector (Fig. 2), where the extent of the obstacle-free fetch is large enough for the the IBL to reach the 20-m level. For most directions the present data set is too coarse to do a detailed analysis of the IBL-structure of the Cabauw site. From earlier research is was found that near-neutral wind speed profiles at Cabauw show a knee around 20 m in the south-west direction, and around 10 m in the east direction. Both the lower and upper part of the profile is logarithmic (Beljaars, 1982). Wieringa (1976) reported that the upper profiles corresponded to the gustiness derived roughness lengths. This is confirmed by Figure 7b.

At Cabauw the friction velocity is routinely computed from the large-scale roughness $z_{0\mathrm{drag}}$ and the wind speed at 10 m. For most directions this method is accurate. However, in the south-west sector the 10-m wind is well within the local IBL. Here the wind speed is adapted to the smooth grass-covered land, whereas the roughness length still represents the high, large-scale average. This results in an overestimation of the friction velocity and hence the wind speed (gradient) as was seen in Nieuwstadt (1978).

Nieuwstadt (1978) compared the friction velocity from his profile method with direct flux measurements at 20 m. The large-scale roughness length $z_{0\mathrm{std}}$ was added to the profile ($U(z_0) = 0$). For most directions the profile u_* and the directly measured u_* were in agreement. However, for the south-west direction the directly measured u_* was smaller than that from the profiles. Nieuwstadt used $z_0 = 0.07$ m for this direction. He suggested that the roughness length used in this direction was too high. Actually, the roughness length Nieuwstadt used was not to high, but it corresponded only to the upper profile and so did the estimated u_*. The 20-m level is within the local IBL in

this direction and the measured u_* does not correspond to the upper profile.

Meteorological research masts are often placed at sites selected for their undisturbed terrain. Therefore the local roughness is usually smaller than the large-scale roughness. Cabauw is such an example, but at Boulder similar results are found (Korrell et al., 1982; Bowen, 2000).

7.3. Roughness footprints

Significant differences in roughness length are found from different height intervals for wind speed profiles, or when the roughness length is computed from the gustiness, turbulence intensity, or the drag coefficient. The differences have to be explained by the differences in footprint between these methods in combination with the inhomogeneities of the Cabauw environment.

The source area for the 10–40 m profile is expected to be similar to those for eddy-covariance measurements done at $\sqrt{z_{\rm high} z_{\rm low}} = 20$ m. Its source area weight function is falling off rapidly at a distance of 0.5–1 km (Horst, 1999). On this scale the Cabauw environment is very disturbed resulting in a very changeable lower profile $z_{0\rm prof}$ (Figure 7a). The $z_{0\rm drag}$ is much less changeable with direction (Figure 7c). Only in the south-west direction, where the IBL over smooth grass encloses the 20-m level, $z_{0\rm drag}$ represents the local roughness of grass. A similar difference in momentum flux between 3.5 and 22.5 m height was found by Beljaars et al. (1983). Later Schmid and Oke (1990) showed that the source area for the 22.5-m level comprises many obstacles upstream, while for the 3.5-m level the source area is much smoother. So, although the footprints of $z_{0\rm drag}$ and the lower $z_{0\rm prof}$ are expected to be similar, the lower $z_{0\rm prof}$ is corrupted by the wind speed at 10 m which will be enclosed in the local IBL in more directions than the 20-m level. The 20-m level $z_{0\rm drag}$ on the other hand, yields local roughness lengths only if the IBL reaches to that level, and yields large-scale roughness lengths otherwise.

From the spectral point of view gusts are the result of the superposition of several eddies of different sizes. Whereas the largest eddies contribute most significantly to σ_u, the gust is also determined by smaller eddies because of the small time scale of gusts. This means that the source area for $z_{0\rm gust}$ may also be a superposition of large-scale and local roughness. Figure 7c shows that $z_{0\rm gust}$ is exceeded by $z_{0\rm drag}$ in directions where nearby roughness is present. In other directions it is comparable to $z_{0\rm std}$. There seems to be a correlation, however, between $z_{0\rm gust}$ and $z_{0\rm drag}$: every peak in $z_{0\rm drag}$ is accompanied by a peak in $z_{0\rm gust}$. So, the footprint of $z_{0\rm gust}$ seems to be superposition of local and

large-scale roughness indeed, and its footprint is larger than that of $z_{0\mathrm{drag}}$.

8. Summary and Conclusions

The findings op this paper show that the k-vanes are capable of measuring momentum fluxes with sufficient accuracy provided that they are not used at low altitudes. However, the k-vanes proved vulnerable to atmospheric electricity and contamination of the bearings supporting the propellers.

Overall this study confirms the conclusions of earlier studies at Cabauw. In addition we have analyzed fluxes and wind profiles along the tower not explored before up to heights of 100 m. The wind speed profiles in the Cabauw environment are disturbed by the rough-to-smooth transition that can be found in all directions eventually. Only in the south-west direction the free-fetch extends so far that the equilibrium boundary layer over the grass covered land reaches high enough to enclose the flux measurements at 20 m.

Except for unstable cases the momentum flux in our data selection shows significant divergence. The heat flux divergence is even more pronounced. Our data set comprises many cases where the measurements are done above the surface layer. In addition, in unstable conditions the entrainment rate can be expected to be large. This is due to our data selection procedure which is in favor of conditions with developing boundary-layers in the morning hours with significant shear. It is reconfirmed that in stable boundary layers the regular flux-profile relationships are valid provided that local scaling is used. Also in unstable conditions it appears that scaling of the profiles with local fluxes works well, even in directions where the upstream terrain causes strong disturbances of the boundary layer.

We analyzed the roughness lengths using three methods. This showed that every method has his own footprint resulting in every different estimates of the roughness length depending on the method used. The roughness lengths derived at Cabauw from wind speed profiles depend strongly on the height range over which the profile is taken. The lower profiles (< 40 m) are disturbed by the IBL caused by the local rough-to-smooth transition. Roughness lengths from these profiles are completely invalid. The higher profile yields roughness lengths that can be considered area-averaged values, provided that the lower measuring points are not disturbed by the local IBL. Gustiness derived roughness lengths seem to aggregate both nearby and distant roughness elements and is often the largest of the roughness estimates examined here. The rough-

ness from drag coefficients exhibits more local characteristics than the gustiness. However, if the drag coefficient is measured above the local IBL it yields roughness values that are close to the large-scale area-average. At inhomogeneous sites like Cabauw the roughness length can be estimated best by measuring the drag coefficient just above the local internal boundary layers. Indirect ways for determining the drag coefficient like measurements of the gustiness or the standard deviation of horizontal wind speed fluctuations give similar results. These methods are less sensitive to local disturbances of the surface layer than profile derived roughness lengths. The latter are easily disturbed by terrain inhomogeneities resulting in unrealistic values for the roughness lengths.

Acknowledgments

This project was undertaken by the Meteorology and Air Quality Section of Wageningen University (WU) in collaboration with the Royal Netherlands Meteorological Institute (KNMI). It was originally initiated under the supervision of Prof. Dr. J. Wieringa. We are indebted to the technical staff of both KNMI (Sjaak Koster and Frans Renes among others), and WU (Bert Heusinkveld and Frits Antonysen among others), for helping setting up the k-vane measurements. Also thanks to the scientific staff of the Atmospheric Research group of KNMI for making available the profile data. Special thanks to Fred Bosveld for providing the data-acquisition software. The investigations were (in part) supported by the Netherlands Organization for Scientific Research (NWO), project no. 750.194.15.

References

Beljaars, A. C. M.: 1982, 'The derivation of fluxes from profiles in perturbed areas'. *Boundary-Layer Meteorol.* **24**, 35–55.

Beljaars, A. C. M.: 1987a, 'The influence of sampling and filtering on measured wind gusts'. *J. Atmos. Oceanic Technol.* **4**, 613–626.

Beljaars, A. C. M.: 1987b, 'On the memory of wind standard deviation for upstream roughness'. *Boundary-Layer Meteorol.* **38**, 95–101.

Beljaars, A. C. M.: 1988, 'The measurement of gustiness at routine wind stations - a review'. In: *WMO-TECO-1988*. Leipzig, pp. 311–316. WMO/TD-No. 222, also Royal Netherlands Meteorological Institute, Sc. Rep., WR 87-11.

Beljaars, A. C. M. and F. C. Bosveld: 1997, 'Cabauw data for the validation of land surface parameterization schemes'. *J. Climate* **10**, 1172–1193.

Beljaars, A. C. M. and A. A. M. Holtslag: 1991, 'Flux parameterization over land surfaces for atmospheric models'. *J. Appl. Meteorol.* **30**, 327–341.

Beljaars, A. C. M., P. Schotanus, and F. T. M. Nieuwstadt: 1983, 'Surface layer similarity under nonuniform fetch conditions'. *J. Clim. Appl. Meteor.* **22**, 1800–1810.

Bowen, B. M.: 2000, 'Near-neutral surface layer turbulence at the Boulder atmospheric observatory tower: evidence of increasing vertical turbulence with height'. *J. Appl. Meteorol.* **39**, 716–724.

De Wit, A. J. W., T. G. C. Van der Heijden, and H. A. M. Thunnissen: 1999, 'Vervaardiging en nauwkeurigheid van het LGN3 grondgebruiksbestand'. DLO-Staring Centrum, Wageningen. in Dutch, 84 pp.

Driedonks, A. G. M. and H. Tennekes: 1984, 'Entrainment effects in the well-mixed atmospheric boundary layer'. *Boundary-Layer Meteorol.* **30**, 75–105.

Dyer, A. J.: 1974, 'A review of flux-profile relationships'. *Boundary-Layer Meteorol.* **7**, 363–372.

Garratt, J. R.: 1992, *The Atmospheric Boundary Layer.* Cambridge: Cambridge University Press. 316 pp.

Grant, A. L. M.: 1991, 'Surface drag and turbulence over an inhomogeneous land surface'. *Boundary-Layer Meteorol.* **56**, 309–337.

Grant, A. L. M. and P. J. Mason: 1990, 'Observations of the Boundary-Layer Structure over Complex Terrain'. *Quart. J. Roy. Meteorol. Soc.* **116**, 159–186.

Højstrup, J.: 1981, 'A simple model for the adjustment of velocity spectra in unstable conditions downstream of an abrupt change in roughness and heat flux'. *Boundary-Layer Meteorol.* **21**, 341–356.

Holtslag, A. A. M.: 1984, 'Estimation of diabatic wind speed profiles from near-surface weather observations'. *Boundary-Layer Meteorol.* **29**, 225–250.

Holtslag, A. A. M. and H. A. R. De Bruin: 1988, 'Applied Modelling of the Nighttime Surface Energy Balance over Land'. *J. Appl. Meteorol.* **27**, 689–704.

Holtslag, A. A. M. and F. T. M. Nieuwstadt: 1986, 'Scaling the atmospheric boundary layer'. *Boundary-Layer Meteorol.* **36**, 201–209.

Horst, T. W.: 1999, 'The footprint for estimation of atmosphere-surface exchange fluxes by profile techniques'. *Boundary-Layer Meteorol.* **90**, 171–188.

Kljun, N., P. Calanca, M. W. Rotach, and H. P. Schmid: 2004, 'A simple parameterisation for flux footprint predictions'. *Boundary-Layer Meteorol.* **112**, 503–523.

Korrell, A., H. A. Panofsky, and R. J. Rossi: 1982, 'Wind profiles at the Boulder tower'. *Boundary-Layer Meteorol.* **22**, 295–312.

Kustas, W. P. and W. Brutsaert: 1986, 'Wind Profile Constants in a Neutral Atmospheric Boundary Layer over Complex Terrain'. *Boundary-Layer Meteorol.* **34**, 35–54.

Monna, W. A. A. and J. G. Van der Vliet: 1987, 'Facilities for research and weather observations on the 213 m tower at Cabauw and remote locations'. Scientific Report WR 87-5, Royal Netherlands Meteorological Institute. 27 pp.

Nieuwstadt, F. T. M.: 1978, 'The computation of the friction velocity u_* and the temperature T_* from temperature and wind velocity profiles by least-square methods'. *Boundary-Layer Meteorol.* **14**, 235–246.

Nieuwstadt, F. T. M.: 1984, 'The turbulent structure of the stable, nocturnal boundary layer'. *J. Atmos. Sci.* **41**, 2202–2216.

Pino, D., J. Vilà-Guerau de Arellano, and P. G. Duynkerke: 2003, 'The contribution of shear to the evolution of a convective boundary layer'. *J. Atmos. Sci.* **60**, 1913–1926.

Rao, K. S., J. C. Wyngaard, and O. R. Coté: 1974, 'The structure of the Two-Dimensional Internal Boundary Layer over a Sudden Change of Surface Roughness'. *J. Atmos. Sci.* **31**, 738–746.

Schmid, H. P. and C. R. Lloyd: 1999, 'Spatial representativeness and the location bias of flux footprints over inhomogeneous areas'. *Agric. Forest Meteor.* **93**, 195–209.

Schmid, H. P. and T. R. Oke: 1990, 'A model to estimate the source area contribution to turbulent exchange in the surface layer over patchy terrain'. *Quart. J. Roy. Meteorol. Soc.* **116**, 965–988.

Sorbjan, Z.: 1986, 'On similarity in the atmospheric boundary layer'. *Boundary-Layer Meteorol.* **34**, 377–397.

Steeneveld, G.-J., A. A. M. Holtslag, and H. A. R. De Bruin: 2005, 'Fluxes and gradients in the convective surface layer and the possible role of boundary-layer depth and entrainment flux'. *Boundary-Layer Meteorol.* **116**, 237 – 252.

Van der Vliet, J. G.: 1998, 'Elf jaar Cabauw-metingen'. Technical Report TR-210, Royal Netherlands Meteorological Institute. in Dutch, 79 pp.

Van Ulden, A. P.: 1978, 'Simple estimates for vertical diffusion from sources near the ground'. *Atmos. Environ.* **12**, 2125–2129.

Van Ulden, A. P. and J. Wieringa: 1996, 'Atmospheric boundary layer research at Cabauw'. *Boundary-Layer Meteorol.* **78**, 39–69.

Verkaik, J. W.: 1998, 'Evaluation of the K-Gill propeller vane'. *J. Atmos. Oceanic Technol.* **15**, 901–915.

Verkaik, J. W.: 2000, 'Evaluation of two gustiness models for exposure correction calculations'. *J. Appl. Meteorol.* **39**, 1613–1626.

Vickers, D. and L. Mahrt: 1999, 'Monin-Obukhov similarity theory in the coastal zone'. In: *Preprints, 13th Symp. on Boundary Layers and Turbulence*. Dallas, TX, pp. 407–410. Amer. Meteorol. Soc.

Wessels, H. R. A.: 1983, 'Distortion of the wind field by the Cabauw meteorological tower'. Scientific Report WR 83-15, Royal Netherlands Meteorological Institute. 34 pp.

Wessels, H. R. A.: 1984, 'Cabauw meteorological data tapes 1973-1984; description of instrumentation and data processing for the continuous measurements'. Scientific Report WR 84-6, Royal Netherlands Meteorological Institute. 23 pp.

Wieringa, J.: 1976, 'An objective exposure correction method for average wind speeds measured at a sheltered location'. *Quart. J. Roy. Meteorol. Soc.* **102**, 241–253.

Wieringa, J.: 1993, 'Representative Roughness Parameters for Homogeneous Terrain'. *Boundary-Layer Meteorol.* **63**, 323–363.

Yumao, X., Z. Chaofu, L. Zhongkai, and Z. Wei: 1997, 'Turbulent structure and local similarity in the tower layer over the Nanjing area'. *Boundary-Layer Meteorol.* **82**, 1–21.

Address for Offprints: Mr. J. W. Verkaik
Royal Netherlands Meteorological Institute (KNMI)
PO Box 201, 3730 AE De Bilt, the Netherlands